Stability of Ru- and Ta-Based Metal Gate Electrodes in Contact With Dielectrics for Si-CMOS

Zhiqiang Chen[*1], Veena Misra[2], Ryan P. Haggerty[1], and Susanne Stemmer[1]**

[1] Materials Department, University of California, Santa Barbara, CA 93106-5050
[2] Department of Electrical Engineering, North Carolina State University, Raleigh, NC 27695-7911

Received zzz, revised zzz, accepted zzz
Published online zzz

PACS 00.00Xx, 11.11.Yy

The Ru-Ta-Si-O, Ta-Si-N-O, and Ru-Ta-Zr-O phase diagrams are important for predicting reactions at interfaces between SiO_2 and ZrO_2 gate dielectrics and novel Ru and Ta-based metal gate electrodes. Simplified quaternary phase diagrams of the Ru-Ta-Si-O, Ta-Si-N-O, and Ru-Ta-Zr-O systems at 900°C were constructed from known and estimated Gibbs free energy data, respectively. Ru is predicted to be stable in contact with ZrO_2 and SiO_2, whereas Ta is not stable in contact with SiO_2 at temperatures around 900 °C. Stoichiometric RuTa and TaN compounds were estimated to be stable in contact with both dielectrics at 900 °C. Experimental observations of gate electrode/dielectric interfaces are discussed. They are consistent with the thermodynamic predictions within the limitations of these phase diagrams. Metastable phases, often found in TaN_x films, and diffusion of species from the vapor (e.g., oxygen), in particular along grain boundaries in columnar gate electrodes, may lead to reactions not predicted by the equilibrium phase diagrams.

1 Introduction

Continued scaling of complementary metal–oxide–semiconductor (CMOS) devices will require a gate dielectric with a capacitance equivalent to that of SiO_2 of less than 1 nm thickness in the near future. As the equivalent oxide thickness (EOT) is decreased, the introduction of oxides with dielectric constants (*k*) greater than that of SiO_2 or silicon oxynitrides will be required to allow physically thicker gate dielectrics with reduced leakage currents. Concurrently, heavily doped polycrystalline Si, presently used as the gate electrode, may have to be replaced with metal gate electrodes [1]. Metal gates are attractive for both SiO_2-based and high-*k* gate dielectrics because they eliminate gate depletion, thus allowing lower EOTs, and are potentially thermally more stable in contact with high-*k* oxides than Si. Furthermore, dopant penetration from polycrystalline Si gate electrodes into the Si channel [2-4] could be eliminated if metal electrodes were used.

Necessary requirements for alternative metal gate electrodes are work functions that are compatible with low threshold voltages and the thermal stability of the interface with the dielectric at device fabrication temperatures. Optimal work functions for *n*-type MOS and for *p*-type MOS must be around 5 eV and 4 eV, respectively. In addition, midgap gate electrodes [5], as well as integration schemes to obtain dual workfunction gates for both types of MOS have been proposed. Integration approaches use, for example, interdiffusion to selectively change the workfunction over one of the devices [6-8]. Ru-Ta alloys are attractive for such schemes because their workfunction can be systematically varied between 4.2 and 5 eV [9] by changing their composition.

With respect to the thermal stability of the candidate metal electrodes in contact with the dielectric, many elemental electrodes are not stable in contact with SiO_2 [10]. These include Zr, Al, Hf, Ti, Nb and Ta [10-13], which are thus unsuitable if SiO_2 is the gate dielectric. However, little is known about the

[*] now at Brookhaven National Laboratory
[**] Corresponding author: e-mail: stemmer@mrl.ucsb.edu, Phone: +001 805 893 6128, Fax: +001 805 893 7221

 0031-8965/03/0101-0003 $ 17.50+.50/0

thermal stability of alloy metal gate electrodes in contact with SiO_2, or even elemental metals in contact with novel high-*k* gate dielectrics such as ZrO_2 and HfO_2. The objective of this study is to investigate the stability of gate electrode stacks using Ru, Ru-Ta alloys, Ta and TaN gate electrodes. To this purpose we have calculated the relevant ternary and quaternary phase diagrams that can be used to predict the thermodynamic stability or interface reactions at these interfaces. Experimental studies of Ru/SiO_2, $Ru/Ta/SiO_2$, $Ru\text{-}Ta/SiO_2$, $Ru/Ta/ZrO_2/SiO_2$ and TaN/SiO_2 interfaces after thermal anneals are also presented.

2 Thermodynamics

Although thin films are not necessarily in equilibrium, ternary or quaternary phase diagrams are an important tool to predict possible reactions between electrodes and dielectric oxides. For an elemental metal electrode, such as Ta or Ru, in contact with a binary gate oxide, such as SiO_2 or ZrO_2, the relevant phase diagram is a ternary system, whereas in case of a compound gate electrode, such as TaN and RuTa, a quaternary system must be employed. BEYERS *et al.* [11,14] and BHANSALI *et al*. [15,16] have developed approaches to construct simplified ternary and quaternary phase diagrams at arbitrary, constant temperature and pressure and have shown that they can be applied to predict thin film reactions or stability. We briefly summarize their method.

In ternary phase diagrams, two phases are thermodynamically stable in contact with each other when a stable tie line exists between them. Stable tie lines can be determined by calculating the Gibbs free energy of reactions involving two reactants and two products that make up the competing tie lines (tie lines cannot cross because at the intersection four phases would be in equilibrium, which is forbidden by the Gibbs phase rule for a ternary system at constant, arbitrary temperature and pressure). If the Gibbs free energy is negative, then the tie line representing the products is stable. For example, in the Ta-Si-O phase diagram (Fig. 1(a)), a possible tie line between Ta_2O_5 and Ta_2Si is determined by calculating the Gibbs free energy change of reactions involving possible competing tie lines, for example:

$$14Ta + 5SiO_2 \rightarrow 2Ta_2O_5 + 5Ta_2Si \qquad (1)$$

For each of these reactions, $\Delta G^{\circ}_{900°C}$ is the change in Gibbs free energy for the reaction at 900 °C, with each of the reactants and products in their standard state. $\Delta G^{\circ}_{900°C}$ of reaction (1) is ~ -214 kJ/mol. The negative value indicates that the reaction proceeds in the direction indicated, i.e., Ta has driving force to react with SiO_2 to form Ta_2O_5 and Ta_2Si, i.e. there is no tie line between SiO_2 and Ta.

A quaternary system can be represented by a tetrahedron with its faces representing the four ternary systems that make up the quaternary. Tie lines can be external (connecting phases in the ternary phase diagrams) or internal, i.e., inside the tetrahedron, joining phases on opposite sides of the tetrahedron. In addition, tie planes (bound by three tie lines) represent a three-phase equilibrium. They divide the quaternary phase diagram into non-intersecting tie-tetrahedra. To determine stable tie lines and tie planes in quaternary systems, BHANSALI *et al.* make use of the rule that tie lines and tie planes cannot cross, as this would violate Gibbs phase rule for a four component systems at constant, arbitrary temperature and pressure [16]. The existence or absence of an internal tie line can be determined by calculating the Gibbs free energy changes of reactions involving all possible triangles that intersect the tie line in question. Homogeneity ranges are not shown in such simplified phase diagrams, but do not compromise the validity of conclusions about the stability of the phases in contact with each other [11]. Most systems under consideration have a strong tendency to form compounds as opposed to solid solutions.

In the following section, we develop such phase diagrams to predict the stability of Ru, Ta, TaN and RuTa in contact with SiO_2 and ZrO_2, respectively. ZrO_2 is one of the candidate dielectrics currently investigated to replace SiO_2. We use free energies at 900 °C, but predictions are expected to be valid within a few 100 K, as free energy differences do not change much over this range. Thermodynamic data were obtained from ref. [17], unless stated otherwise. The data in ref. [17] is often reported with a large number of significant digits. However, there is great uncertainty in some of the data and we report

all data only to three significant digits. In cases when estimates were used, as described below, the uncertainty may be greater than 10%.
For thin layers, gaseous species may diffuse through the gate electrode, leading to interfacial reactions not predicted by the thermodynamic stability analysis described above. For example, oxygen diffusing through a thin layer may cause the formation SiO_2 by oxidation of the Si surface. We discuss such reactions in sections 3 and 4.

2.1 The Ru-Ta-Si-O system

The phase diagram for the quaternary Ru-Ta-Si-O system is necessary to evaluate the stability of RuTa compounds on SiO_2. The four isothermal (900 °C) ternary systems, Ta-Si-O, Ru-Si-O, Ta-Si-Ru, and Ta-Ru-O, make up the Ru-Ta-Si-O diagram. The Ta-Si-O and Ru-Si-O phase diagrams predict the thermodynamic stability of Ta and Ru, respectively, on SiO_2. They have been published previously [11,13,18,19]. The calculated Ta-Si-O phase diagram at 900 °C is shown in Fig. 1(a) is identical to that shown in ref. [11]. The Gibbs free energies of phases in the Ru-Si-O system at 900°C are given in Table 2. They were obtained from ref. [17], with the exception of the ruthenium silicides, which were calculated using the optimized thermodynamic parameters given in ref. [20]. The calculated Ru-Si-O phase diagram at 900 °C is shown in Fig. 1(b). It includes Ru_2Si, which was not included by GASSER [18]. The phase diagram predicts that Ru is stable in contact with SiO_2 since there is a tie line between them.

Ru-Ta-Si and Ru-Ta-O

The Gibbs free energies of the compounds between Ru and Si and between Ta and Si are shown in Tables 1 and 2.

Table 1 Standard Gibbs free energies of the different compounds and elements in the Ta-Si-O system at 900 °C [17].

Phase	Gibbs free energy (kJ/mol)
Ta	-67.9
Si	-39
Ta_2Si	-304
Ta_5Si_3	-808
$TaSi_2$	-239
O_2	-263
Ta_2O_5	-2330
SiO_2	-1000

Table 2: Standard Gibbs free energies of the compounds and elements in the Ru-Si-O system at 900 °C [17,20].

Phase	Gibbs free energy (kJ/mol)
Ru	-52
Ru_2Si_3	-505
RuSi	-207
Ru_4Si_3	-698
Ru_2Si	-263
RuO_2	-427

The Ru-Ta binary phase diagram contains several compounds around the equiatomic $Ru_{50}Ta_{50}$ composition that are believed to be distorted CsCl type structures [21,22]. No experimental Gibbs free energy values exist in literature for these compounds. Several authors have estimated the formation

enthalpy of RuTa [23-25]. Estimations by KAUFMAN *et al.* were optimized using experimental phase diagrams [25] and are used here. The enthalpy of RuTa at a given temperature can be estimated as follows [25]:

$$H_{RuTa}[T] = (1-x)\,H^{\circ}_{Ru}[T] + xH^{\circ}_{Ta}[T] + \Delta H^{f}_{RuTa}[298K] \quad (2)$$

where x corresponds to atom percent of Ta in RuTa, $H^{\circ}_{Ru}[T]$ and $H^{\circ}_{Ta}[T]$ are the enthalpy of formation of Ru and Ta, respectively, at temperature T. $\Delta H^{f}_{RuTa}[298K]$ is the formation enthalpy of RuTa at 298 K, as estimated by KAUFMAN [25]. The entropy of RuTa is given by [25]:

$$S_{RuTa}[T] = (1-x)S^{\circ}_{Ru}[T] + xS^{\circ}_{Ta}[T] \quad (3)$$

where $S^{\circ}_{Ru}[T]$ and $S^{\circ}_{Ta}[T]$ are the entropy of Ru and Ta, respectively, at temperature T. Using eqs. (2) and (3), the Gibbs free energy of RuTa, ΔG°_{RuTa} at 900 °C is estimated to be about -235 kJ/mol. Only stoichiometric RuTa is considered here, although this compound has extensive solubility for both Ru and Ta [22]. The calculated Ru-Ta-Si phase diagram at 900 °C is shown in Fig. 1(c).
The isothermal Ru-Ta-O phase diagram at 900 °C is shown in Fig. 1 (d). Note that RuTa is predicted to react with O, as there is no tie line between them.

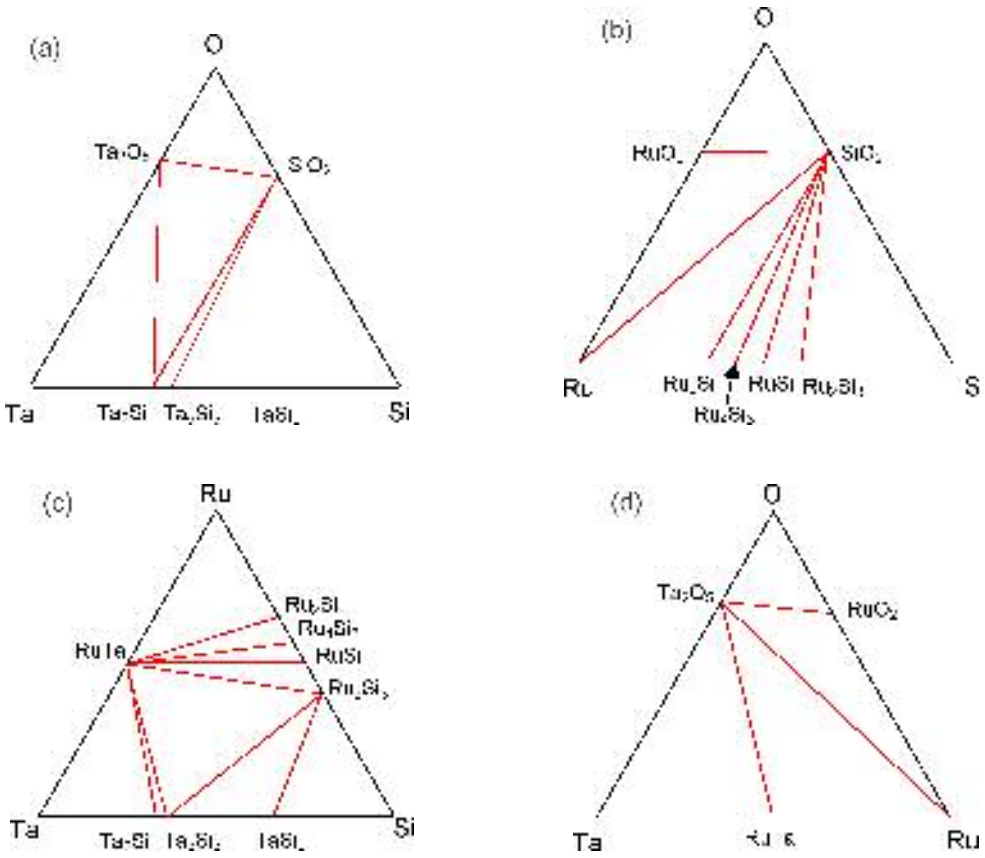

Fig. 1 Calculated tie lines in the ternary phase diagrams of the (a) Ta-Si-O, (b) Ru-Si-O, (c) Ru-Ta-Si, and (d) Ru-Ta-O systems at 900 °C.

Ru-Ta-Si-O

Possible tie triangles in the quaternary Ru-Ta-Si-O phase diagram that can be constructed from the external tie lines are Ta_2O_5-RuTa-Ta_2Si, Ta_2O_5-SiO_2-Ru, Ta_2O_5-SiO_2-RuO_2, SiO_2-Ta_5Si_3-Ru_2Si_3, SiO_2-$TaSi_2$-Ru_2Si_3. Possible internal tie lines are Ta_2O_5-Ru_2Si, Ta_2O_5-Ru_4Si_3, Ta_2O_5-RuSi, Ta_2O_5, Ru_2Si_3, RuO_2-Ta_2Si, RuO_2-Ta_5Si_3, RuO_2-$TaSi_2$ and SiO_2-RuTa.
The existence of the RuTa-SiO_2 tie line can be determined by calculating the Gibbs free energy changes of reactions involving all possible triangles that intersect with RuTa-SiO_2 [16]. The reactions and free energy changes that establish RuTa-SiO_2 as an internal tie line are listed in the Appendix. All other possible internal tie lines could be eliminated by calculation of Gibbs free energy changes of the reactions involving intersecting tie triangles (see Appendix), which also confirmed the tie triangles shown in Fig. 2, which represents the complete Ru-Ta-Si-O quaternary phase diagram. The bold dashed line indicates the internal RuTa-SiO_2 tie line in the quaternary system, which indicates that RuTa gate electrodes may be stable in contact with SiO_2. More accurate predications could be made if the free energy of formation of the different phases in the Ru-Ta phase diagram were determined experimentally. Due to the uncertainty in the free energy of RuTa, experimental results are shown in section 3.

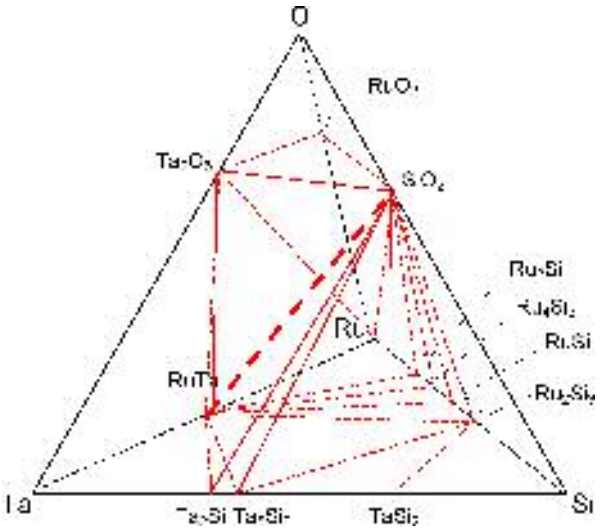

Fig. 2: Calculated quaternary phase diagrams of the Ru-Ta-Si-O system at 900 °C. The solid or dashed lines represent the tie lines on the faces of the tetrahedron, and the bold dashed line is the interior SiO_2-RuTa tie line. The phase diagram is not drawn in correct perspective.

2.2 The Ta-Si-N-O system

The quaternary Ta-Si-N-O system is needed to determine the thermodynamic stability of TaN in contact with SiO_2. The four ternary phase diagrams that make up the quaternary system are Ta-Si-N, Si-N-O, Ta-Si-O, and Ta-N-O. The free energies are listed in Tables 3 and 4 and the free energy changes are listed in the Appendix. The Ta-N system is very complex, because in addition to the two equilibrium nitrides that are considered here, TaN and Ta_2N, a number of metastable phases are known to exist. There is a lack of thermochemical information for these phases, and they were not included in the calculations presented below. Their presence may potentially alter conclusions regarding stability in this system, as will be discussed in section 3.

Table 3: Standard Gibbs free energies of elements and compounds in the Ta-Si, Ta-N, and Si-N systems at 900 °C [17,33]. Given in parenthesis are calculated values from ref. [52], but were not used here.

Phase	Gibbs free energy (kJ/mol)
N_2	-247
TaN	-349 (-328)
Ta_2N	-428 (-395)
Si_3N_4	-1000

Table 4: Gibbs free energies of elements and compounds in the Si-N-O system at 900 °C [17,33].

Phase	Gibbs free energy (kJ/mol)
SiO_2	-1000
Si_2N_2O	-1050

Ta-Si-N

LEE *et al.* [26] have calculated the Ta-Si-N ternary phase diagram using BEYERS method and Gibbs free energy data from BARIN [17] (Fig. 3(a)). LEE *et al.* showed that there was no change in the stable tie lines between 300 and 1700 K. Note that Si and TaN will react, as the following reaction has a negative free energy change (see Appendix):

$$11\mathrm{Si} + 4\mathrm{TaN} \rightarrow \mathrm{Si_3N_4} + 4\mathrm{TaSi_2} \quad (4)$$

Ta is not a suitable gate electrode if Si_3N_4 were used as the gate dielectric as no tie line exists between the two phases. It should be noted that an experimental Ta-Si-N phase diagram published in literature shows a tie line between Ta_2N and Si_3N_4 at 1000 °C [27]. Furthermore, Ta_3Si [28] and Ta_4Si [29] have been reported but were not included in the calculations here, due to lack of thermodynamic data. However, these compounds likely do not significantly change the phase diagram shown [27].

Si-O-N

The Si-N-O system contains a ternary compound, Si_2N_2O [30-32]. The free energies of Si_2N_2O and Si_3N_4 were obtained from ref. [33]:

$$\Delta G^{\circ}_{\mathrm{Si_2N_2O}} = -966832 + 731.008 \cdot T - 111.7238 \cdot T \cdot \ln T - 0.005872 \cdot T^2 - 2185000/T \quad (5)$$

$$G^{\circ}_{Si_3N_4} = -936806 + 1066.040 \cdot T - 158.4527 T \cdot \ln T - 0.008226 \cdot T^2 + 10886000/T - 773000000/T^2 \quad (6)$$

The calculated Si-N-O phase diagram is shown in Fig. 3(b).

Ta-N-O

Ternary compounds have been reported in this system [34]. However, no thermodynamic or structural data are available for these compounds. Therefore, the Ta-N-O phase diagram at 900 °C was calculated without considering these compounds and is shown in Fig. 3(c).

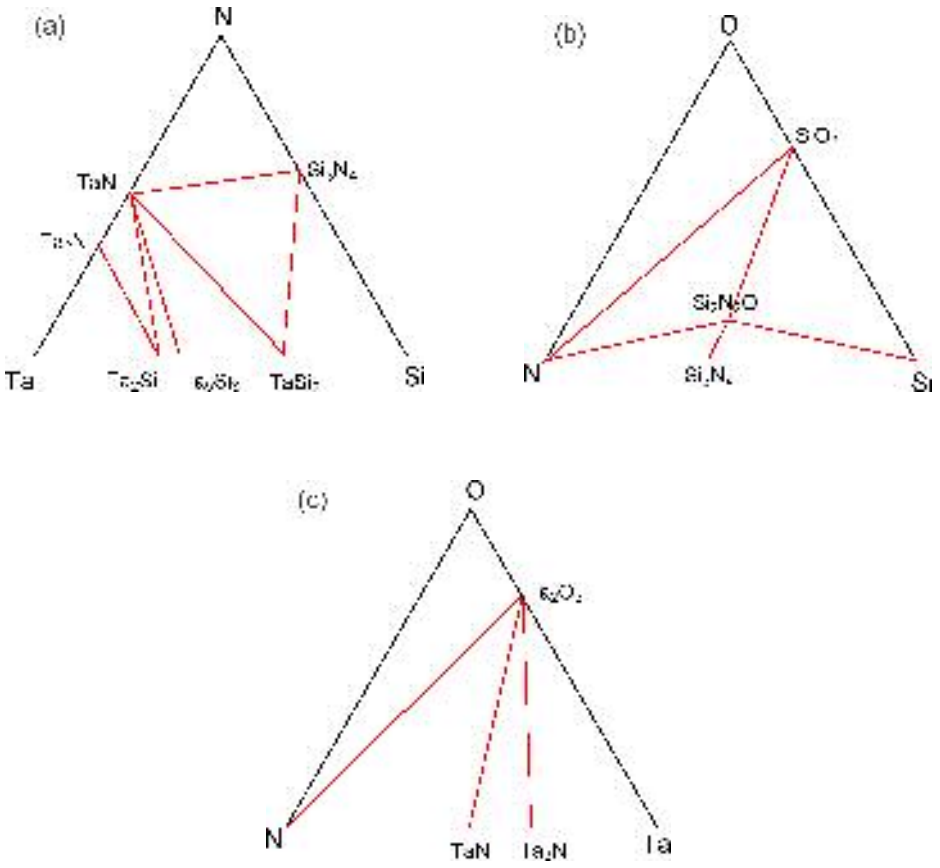

Fig. 3: Calculated tie lines in the ternary phase diagrams of the (a) Ta-Si-N, (b) Si-N-O, and (c) Ta-N-O systems at 900 °C.

Ta-Si-N-O

The possible tie triangles that can be constructed from the external tie lines for the quaternary Ta-Si-N-O phase diagram are Ta_2O_5-Ta_2N-Ta_2Si, Ta_2O_5-TaN-Ta_2Si and Ta_2O_5-SiO_2-N_2. TaN-SiO_2 and $TaSi_2$-Si_2N_2O were established as internal tie lines by the evaluation of Gibbs free energy changes for all possible reactions involving crossing tie lines and tie planes. The calculated Ta-Si-N-O quaternary phase diagram is shown in Fig. 4. The bold dashed lines indicate the internal tie lines; all other lines indicate tie triangles. Note that the existence of Ta_2O_5-Si_3N_4 and Ta_2O_5-Si_2N_2O tie lines was ruled out based on reaction involving N_2 as a product. Such reactions are unlikely if solid-solid interfaces are considered, unless N_2 gas can escape, for example by diffusion through a thin layer. Therefore, a thick Ta_2O_5 film is likely stable in contact with a thick Si_3N_4 or Si_2N_2O layer. The Ta-Si-N-O quaternary phase diagram shows that stoichiometric TaN will be stable in contact with SiO_2, while Ta_2N, which has been considered as a gate electrode [35], will react with SiO_2.

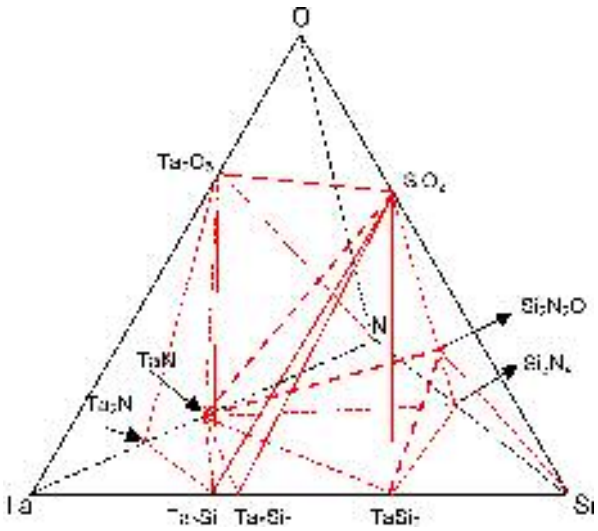

Fig. 4: Calculated quaternary phase diagram of the Ta-Si-N-O system at 900 °C. The solid or dashed lines represent the tie lines on the faces of the tetrahedron. The internal tie lines are shown as bold dashed lines. An internal tie line exits between TaN and SiO_2 but no tie line exists between Ta_2N and SiO_2. The external tie lines between TaN, SiO_2 and$TaSi_2$ do not form an internal tie triangle. The phase diagram is not drawn in correct perspective.

2.3 The Ru-Ta-Zr-O system

The Ru-Ta-Zr-O phase diagram is important to determine whether RuTa is stable at 900 °C in contact with ZrO_2, which is currently considered as an alternative gate dielectric. The Gibbs free energies of RuZr and Ru_2Zr were estimated from the values given by MAHDOUK *et al.* [36] using the following equations

$$\Delta G_{RuZr}[1173.15\mathrm{K}] = 2\left(0.5G_{Ru}[1173.15\mathrm{K}] + 0.5G_{Zr}[1173.15\mathrm{K}] + \Delta H_f - 1173.15\Delta S_f\right) \quad (7)$$

$$\Delta G_{RuZr}[1173.15\mathrm{K}] = 3\left(0.6667G_{Ru}[1173.15\mathrm{K}] + 0.3333G_{Zr}[1173.15\mathrm{K}] + \Delta H_f - 1173.15\Delta S_f\right) \quad (8)$$

where G_{Ru} and G_{Zr} are the free energy values listed in the tables and ΔH_f and ΔS_f were obtained from MAHDOUK *et al.* (-55.8 kJ/mol and 8.9 J/Kmol, respectively for RuZr and –32.08 kJ/mol and 9.5 J/Kmol, respectively for Ru_2Zr). These estimated values were used to calculate the Ru-Zr-Ta and Ru-Zr-O ternary phase diagrams shown in Figs. 5(a-b). The ternary Ta-O-Zr phase diagram is shown in Fig. 5 (c). There are no compounds in the binary Ta-Zr system [37]. In contrast to SiO_2, Ta is predicted to be stable in contact with ZrO_2. Thus Ta may be a suitable gate electrode for alternative gate dielectrics. The quaternary phase diagram Ru-Ta-Zr-O, shown in Fig. 6, exhibits an internal tie line between RuTa and ZrO_2, which implies that RuTa is stable in contact with ZrO_2.

Table 5: Gibbs free energies of elements and compounds in Zr-O and Ru-Zr systems at 900 °C [17,36].

Phase	Gibbs free energy (kJ/mol)
Zr	-65.4
ZrO_2	-1210
RuZr	-250
Ru_2Zr	-299

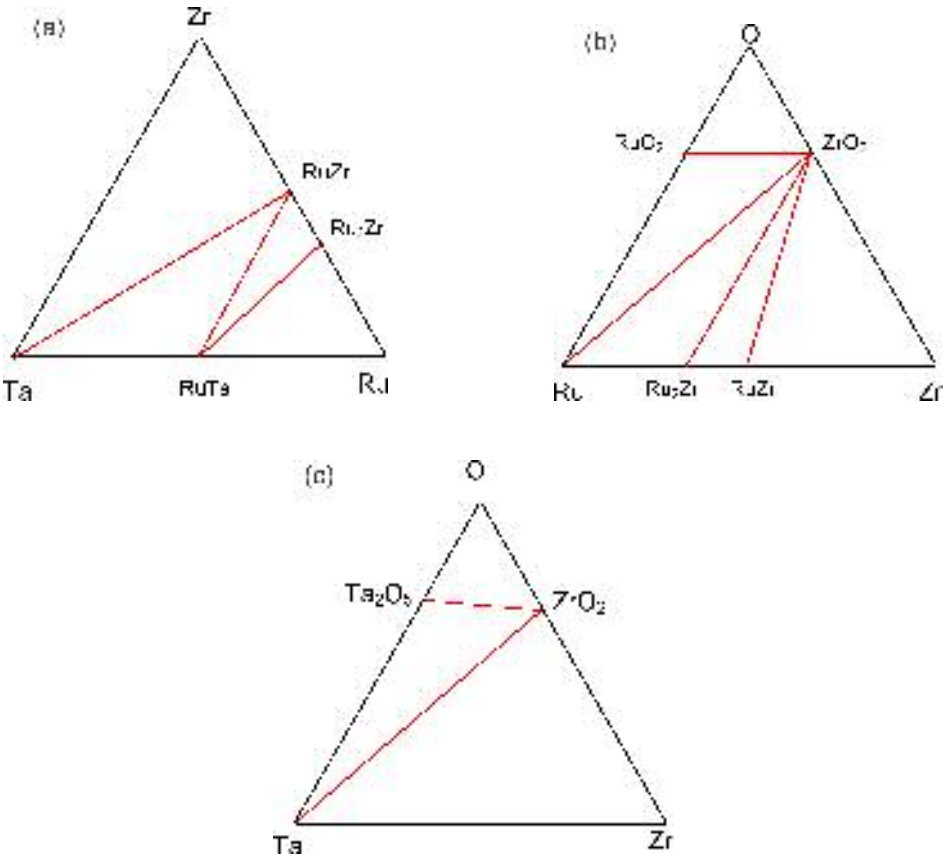

Fig. 5: Calculated tie lines in the ternary phase diagrams of the (a) Ru-Ta-Zr, (b) Ru-Zr-O, and (c) Ta-Zr-O systems at 900 °C.

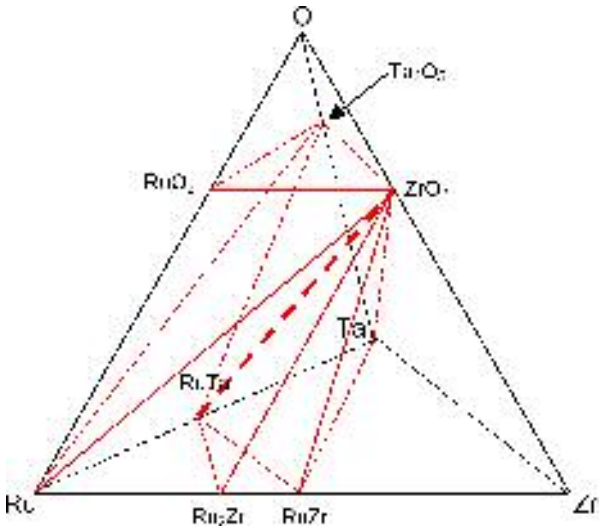

Fig. 6: Calculated quaternary phase diagrams of the Ta-Si-N-O system at 900 °C. The internal tie line is shown as a bold dashed line. The phase diagram is not drawn in correct perspective.

3. Experimental Results

To experimentally evaluate metal gate electrode/dielectric interface stability, Ru, Ru/Ta bilayers and Ru-Ta alloy thin films were deposited on thermally grown SiO_2 and physically vapor deposited ZrO_2, respectively, by sputtering. The details of sputtering process are described elsewhere [9]. The composition of the Ru-Ta alloy was approximately 40 at% Ta. After deposition, the electrodes were patterned using lift-off and annealed at 400 °C for 30 min in forming gas ($10\%H_2/N_2$), followed by a rapid thermal anneal at 900 °C in N_2 for 30 s. TaN films were deposited by reactive sputtering from a Ta target using a 1:5 N_2/Ar sputter gas mixture. Samples for transmission electron microscopy (TEM) were prepared by standard cross-section techniques with Ar ion milling as the final step. The film microstructure were investigated using a 200 kV transmission electron microscope (JEOL JEM 2010F) equipped with a field-emission gun.

Figure 7 shows high-resolution TEM (HRTEM) micrographs of Ru/SiO_2 (Fig. 7 a), Ta/SiO_2 (Fig. 7 b), Ta/ZrO_2 (Fig. 7 c), and $RuTa/SiO_2$ (Fig. 7 d) interfaces recorded along $<110>_{Si}$ after annealing at 900 °C. The Ta/SiO_2 interface shows a thick (~ 3nm), amorphous reaction layer, consistent with the predictions of thermodynamic instability of this interface. The initial SiO_2 thickness underneath this stack was ~ 3nm. SiO_2 was consumed by the interfacial reaction, so that only ~ 1.5 nm SiO_2 layer is left after annealing. The possible reaction products (Fig. 1(a)) are Ta_2Si and Ta_2O_5 because an imaginary tie line between Ta and SiO_2 would intersect the tie line connecting these two phases. Since the reaction product is amorphous, it is experimentally the very difficult to distinguish between the different phases that may be present. The instability of this interface is consistent with observations [13] and predictions [10] by others.

No obvious reaction layers can be detected at Ru/SiO_2, Ta/ZrO_2, and $RuTa/SiO_2$ interfaces, consistent with the predictions of thermodynamic stability as well as previous observations [38]. The thickness of the SiO_2 layer underneath the Ru electrode is about 3.8 nm, compared with an as-deposited thickness of about 3 nm. An increase in SiO_2 thickness during annealing process is likely due to oxygen diffusion through the metal and oxidation of silicon substrate. Oxygen partial pressures during annealing in N_2 are sufficient to cause oxidation of the Si interface [39,40], and SiO_2 growth is controlled by the oxygen diffusivity through the gate electrode. Oxygen diffusion through the grain boundaries of electrodes has been observed for several gate electrodes, including Ru [41]. The Ru electrode has a columnar grain structure, which may facilitate oxygen transport to the interface. Low magnification TEM micrographs showed an increase in thickness of the SiO_2 film in the vicinity of grain boundaries (see inset in Fig 7(a)). RuTa electrodes had smaller grain sizes than Ru electrodes and Ta has a higher affinity with O than Ru. Both may contribute to the oxygen diffusivity through this electrode.

Figure 8 shows HRTEM micrographs of interfaces between N-rich TaN_x films and SiO_2, recorded along <110> Si. One sample (Fig. 8(a)) was annealed at 400°C for 30 min in forming gas ($10\%H_2/N_2$). The other sample was annealed at 1000 °C for 15s in Ar, followed by the same forming gas anneal (Fig. 8(b)). The SiO_2 thickness in both stacks is about 2.7-3.0 nm. There are no apparent reaction layers, confirming the thermal stability of this interface. However, further studies are needed to investigate the degree of N-diffusion from the gate electrode into the dielectric.

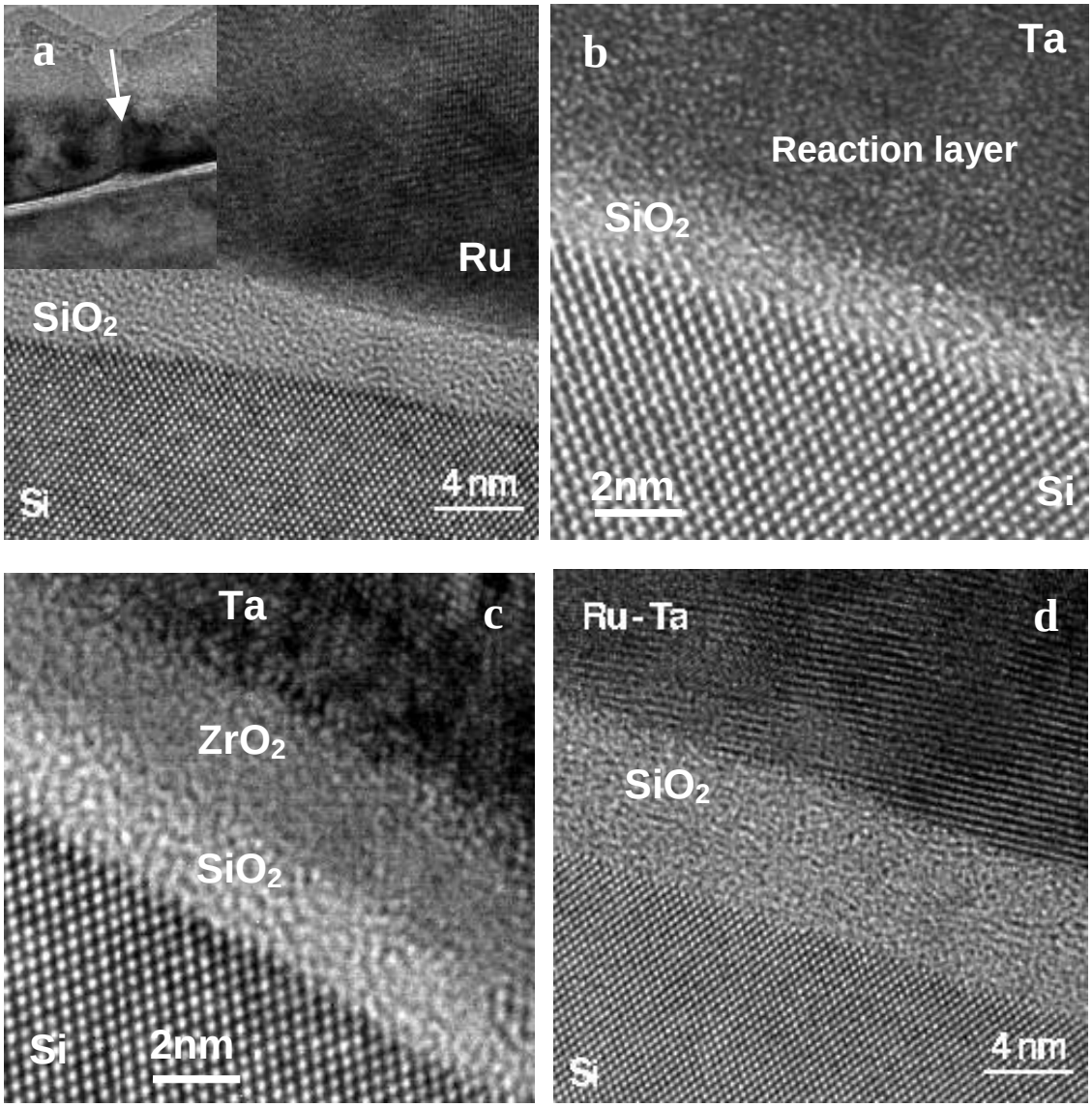

Fig. 7: HRTEM micrographs of interfaces of (a) $Ru/SiO_2/Si$, b) $Ru\text{-}Ta/SiO_2/Si$, (c) $Ta/ZrO_2/SiO_2/Si$, and (d) $Ta/SiO_2/Si$ annealed at 900 °C for 30s. The inset in (a) shows a low magnification micrograph of the Ru film. The arrow indicates a grain boundary and increased SiO_2 thickness in the vicinity of the grain boundary. Note the amorphous reaction layer for the Ta film on SiO_2 (the Ta film is only visible at the top-right corner of the image) and the abrupt, crystalline Ta interface on ZrO_2.

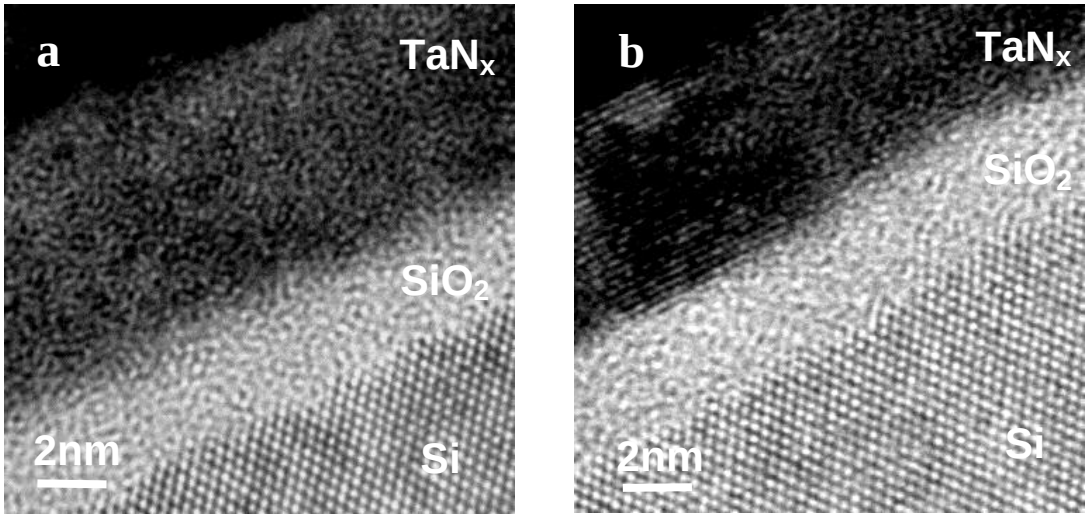

Fig. 8: HRTEM micrographs of a N-rich TaN_x film on SiO_2/Si heat treated at (a) 400 °C (30 min) and (b) 1000 °C/15 s.

4 Discussion

Both HRTEM and thermodynamic estimates in this study indicate that TaN and RuTa are thermally stable at 900 °C in contact with SiO_2 and a high-*k* dielectric, ZrO_2. In contrast, Ta_2N is predicted not to be stable in contact with SiO_2, consistent with recent experimental observations [42]. TaN has been shown to be thermally stable on HfO_2 up to 900 °C [43]. Data from electrical measurements indicate a limited stability range of TaN metal electrodes [35,44]. Capacitance-voltage (CV) measurements of $Si/SiO_2/TaN_x$ structures using N-deficient TaN_x films show a reduced capacitance density after annealing whereas N-rich films showed no changes [45]. The fact that Ta_2N is not stable in contact with SiO_2 may explain some of the observations. N diffusion into the SiO_2 or HfO_2 was also observed at high temperatures [8,43]. Furthermore, while the Ta-N equilibrium phase diagram shows only the nitrides that were included in the calculations for Fig. 4, a great number of metastable phases are known to exist in this system. The phase composition of vapor deposited films is determined by the growth conditions [46]. For example, the Ta_3N_5 phase is often observed in vapor deposited films [35,47,48]. These metastable phases may have different stabilities in contact with SiO_2. Changes in the electrical properties of the gate stack may also be due to changes in the concentration of Ta vacancies, which likely depend on the annealing conditions and which influence the electrical properties of TaN_x electrodes [49].

5 Conclusions

In summary, we have used ternary and quaternary phase diagrams to evaluate the thermodynamic stability of several Ta- and Ru-based metal gate electrodes in contact with SiO_2 and ZrO_2, respectively. The method can be applied to other candidate electrodes and dielectrics, if thermodynamic data are available. Ta is predicted to be not stable in contact with SiO_2 during thermal processing at ~ 900 °C, but is stable in contact with ZrO_2. Ru, stoichiometric RuTa and stoichiometric TaN are predicted to be stable in contact with both gate dielectrics. Experimental investigations of the interface structure are consistent with the predictions, although electrical measurements have implied stability problems for some of the gate electrodes. Oxygen diffusion through the gate electrode and subsequent oxidation of the Si interface may be an issue for several candidate metals, as are metastable and ternary phases that were not included in the calculations of the simplified phase diagrams presented here.

Acknowledgements This research was supported by the SRC/Sematech Front End Process Center. The authors thank Drs. Huicai Zhong and Greg P. Heuss for the deposition of the gate electrodes. We also thank Ms. Yan Yang for help with the TEM sample preparation, Mr. Alexey A. Romanov Jr. for help with the calculations and Prof. Carlos Levi of UCSB for discussions. One of the authors (Z. Q. C.) thanks Prof. M. Hillert of the KTH-Royal Institute of Technology (Sweden) and Dr. Z. -K. Liu of Penn Sate University for valuable discussions. R.P.H. acknowledges support through a UCSB MRL undergraduate RISE fellowship.

References

1. International Technology Roadmap for Semiconductors <http://public.itrs.net/HomeStart.htm> (2003).
2. T. Aoyama, K. Suzuki, H. Tashiro, Y. Toda, T. Yamazaki, K. Takasaki, and T. Ito, J. Appl. Phys. **77,** 417 (1995).
3. T. Brozek, C. Kyono, and V. Ilderem, Solid-State Electronics **45,** 1293 (2001).
4. G. Innertsberger, T. Pompl, and M. Kerber, Microelectron. Reliability **41,** 973 (2001).
5. D. A. Buchanan, F. R. McFeely, and J. J. Yurkas, Appl. Phys. Lett. **73,** 1676 (1998).
6. I. Polishchuk, P. Ranade, and T.-J. King, IEEE Electron Device Lett. **23,** 200 (2002).
7. V. Misra, H. C. Zhong, and H. Lazar, IEEE Electron Device Lett. **23,** 354 (2002).
8. V. Misra, G. Lucovsky, and G. Parsons, MRS Bull. **27,** 212 (2002).
9. H. Zhong, S.-N. Hong, Y.-S. Suh, L. H., H. G., and M. V., IEDM Tech. Digest**,** 467 (2001).
10. R. Pretorius, J. M. Harris, and M. A. Nicolet, Solid-State Electronics **21,** 667 (1978).
11. R. Beyers, J. Appl. Phys. **56,** 147 (1984).
12. V. Misra, G. P. Heuss, and H. Zhong, Appl.Phys. Lett. **78,** 4166 (2001).
13. T. Ushiki, K. Kawai, I. Ohshima, and T. Ohmi, IEEE Trans. Electron Dev. **47,** 2201 (2000).
14. R. Beyers, R. Sinclair, and M. E. Thomas, J. Vac. Sci. Technol. B **2,** 781 (1984).
15. A. S. Bhansali, D. H. Ko, and R. Sinclair, J. Electron. Mater. **19,** 1171 (1990).
16. A. S. Bhansali, R. Sinclair, and A. E. Morgan, J. Appl. Phys. **68,** 1043 (1990).
17. I. Barin, *Thermochemical Data of Pure Substances*, third ed. (Verlag Chemie, Weinheim, 1995).
18. S. M. Gasser, E. Kolawa, and M. A. Nicolet, J. Appl. Phys. **86,** 1974 (1999).
19. A. Pisch and C. Bernard, Calphad **25,** 639 (2001).
20. Y. Q. Liu, G. Shao, and K. P. Homewood, J. Alloys Compounds **320,** 72 (2001).
21. M. A. Schmerling, B. K. Das, and D. S. Lieberman, Metall. Trans. **1,** 3273 (1970).
22. B. H. Chen and H. F. Franzen, J. Less. Common. Metals **157,** 37 (1990).
23. C. Colinet, A. Pasturel, and P. Hicter, Calphad **9,** 71 (1985).
24. F. R. d. Boer, R. Boom, W. C. M. Mattens, A. R. Miedema, and A. K. Niessen, in *Cohesion in Metals: Transition Metals Alloys* (Elsevier Science, Amsterdam, 1988), p. 446.
25. L. Kaufman and H. Bernstein, *Computer Calculation of Phase Diagrams* (Academic Press, New York, 1970).
26. Y. J. Lee, B. S. Suh, S. K. Rha, and C. O. Park, Thin Solid Films **320,** 141 (1998).
27. *Phase Diagrams of Ternary Boron Nitride and Silicon Nitride Systems*; *Vol.*, edited by P. Rogl and J. C. Schuster (ASM, Materials Park, 1992).
28. F. A. Shunk, *Constitution of Binary Alloys, Second Supplement*(McGraw -Hill, New York, 1969).
29. J. D. H. Donnay and H. M. Ondik, *Crystal data determinative tables*, Vol. 2, second ed. (National Bureau of Standards, 1973).
30. P. Rocabois, C. Chatillon, and C. Bernard, J. Amer. Ceram. Soc. **79,** 1361 (1996).
31. M. B. Fegley, J. Amer. Ceram. Soc. **64,** C124 (1981).
32. V. I. Koshchenko and Y. K. Grinberg, Inorganic Materials **18,** 884 (1982).
33. M. Hillert, S. Jonson, and B. Sundman, Z. Metallkunde **83,** 648 (1992).
34. N. Schonberg, Acta Chem. Scand. **8,** 620 (1954).
35. B. Y. Tsui and C. F. Huang, J. Electrochem. Soc. **150,** G22 (2003).
36. K. Mahdouk, K. Elaissaoui, J. Charles, L. Bouirden, and J. C. Gachon, Intermetallics **5,** 111 (1997).
37. O. K.-V. Goldbeck, Atomic Energy Review **Sp. Iss. 6,** 67 (1976).
38. H. C. Zhong, G. Heuss, Y. S. Suh, V. Misra, and S. N. Hong, J. Electron. Mater. **30,** 1493 (2001).
39. S. Stemmer, Z. Chen, R. Keding, J.-P. Maria, D. Wicaksana, and A. I. Kingon, J. Appl. Phys. **92,** 82 (2002).
40. J. J. Lander and J. Morrison, J. Appl. Phys. **33,** 2089 (1962).
41. A. Grill, W. Kane, J. Viggiano, M. Brady, and R. Laibowitz, J. Mater. Res. **7,** 3260 (1992).
42. C. Cabral, C. Lavoie, A. S. Ozcan, R. S. Amos, V. Narayanan, E. Gousev, J. L. Jordan-Sweet, and J. M. E. Harper, in *Evaluation of CMOS Gate Metal Materials Using In Situ X-Ray Characterization*, Paris, 2003.

43. J. K. Schaeffer, S. B. Samavedam, D. C. Gilmer, V. Dhandapani, P. J. Tobin, J. Mogab, B. Y. Nguyen, B. E. White, S. Dakshina-Murthy, R. S. Rai, Z. X. Jiang, R. Martin, M. V. Raymond, M. Zavala, L. B. La, J. A. Smith, R. Garcia, D. Roan, M. Kottke, and R. B. Gregory, J.Vac. Sci. Technol. B **21,** 11 (2003).
44. G. P. Heuss, H. Zhong, and V. Misra, in *Selection of Metal Gate Electrodes for High-K Dielectrics*, 2000.
45. G. Heuss and V. Misra, (unpublished).
46. C. S. Shin, Y. W. Kim, D. Gall, J. E. Greene, and I. Petrov, Thin Solid Films **402,** 172 (2002).
47. K. Radhakrishnan, N. G. Ing, and R. Gopalakrishnan, Mater. Sci. Eng. B **57,** 224 (1999).
48. K. Baba and R. Hatada, Surf. Coat. Technol. **84,** 429 (1996).
49. C. Stampfl and A. J. Freeman, Phys. Rev. B **67,** art. no. (2003).
50. C. Cabral, V. Misra, and J. C. Lee, unpublished.
51. D. S. Wuu, C. C. Chan, and R. H. Horng, J. Vac. Sci. Technol. A **17,** 3327 (1999).
52. K. Frisk, J. Alloys Compd. **278,** 216 (1998).

Appendix

Reactions and their Gibbs free energy changes for the ternary and quaternary systems depicted in Figs. 1-6 at 900 °C.

Reaction	ΔG (kJ/mol)
Ta-Si-O	
$2Ta_2O_5 + 2SiO_2 \rightarrow 7O_2 + 2Ta_2Si$	4210
$10Ta_2O_5 + 12SiO_2 \rightarrow 37O_2 + 4Ta_5Si_3$	22300
$2Ta_2O_5 + 8SiO_2 \rightarrow 13O_2 + 4TaSi_2$	8300
$5SiO_2 + 2Ta_2Si \rightarrow 2Ta_2O_5 + 7Si$	692
$2Ta_2O_5 + 5Ta_2Si \rightarrow 14Ta + 5SiO_2$	214
$37Ta_2Si + 5SiO_2 \rightarrow 2Ta_2O_5 + 14Ta_5Si_3$	310
$13Ta_2Si + 15SiO_2 \rightarrow 6Ta_2O_5 + 14TaSi_2$	1690
Ru-Si-O	
$RuO_2 + SiO_2 \rightarrow RuSi + 2O_2$	696
$2RuO_2 + 3SiO_2 \rightarrow Ru_2Si_3 + 5O_2$	2040
$4RuO_2 + 3SiO_2 \rightarrow Ru_4Si_3 + 7O_2$	2180
$RuO_2 + 2SiO_2 \rightarrow Ru_2Si + 3O_2$	1380
$Ru + SiO_2 \rightarrow RuO_2 + Si$	588
$2Ru + SiO_2 \rightarrow RuO_2 + RuSi$	472
$7Ru + 3SiO_2 \rightarrow 3RuO_2 + Ru_4Si_3$	1390
$5Ru + 3SiO_2 \rightarrow 3RuO_2 + Ru_2Si_3$	1480
$3Ru + 2SiO_2 \rightarrow 2RuO_2 + Ru_2Si$	1040
Ru-Ta-Si	
$4RuTa + 3Ta_2Si \rightarrow 10Ta + Ru_4Si_3$	474
$RuTa + Ta_2Si \rightarrow 3Ta + RuSi$	128
$2RuTa + 3Ta_2Si \rightarrow 8Ta + Ru_2Si_3$	334
$2RuTa + Ta_2Si \rightarrow 4Ta + Ru_2Si$	238
$RuTa + 5RuSi \rightarrow TaSi_2 + 3Ru_2Si$	243
$5RuTa + 11RuSi \rightarrow Ta_5Si_3 + 8Ru_2Si$	539
$2RuTa + 4RuSi \rightarrow Ta_2Si + 3Ru_2Si$	204
$6RuTa + 5Ru_2Si_3 \rightarrow 3Ta_2Si + 4Ru_4Si_3$	226
$10RuTa + 9Ru_2Si_3 \rightarrow 2Ta_5Si_3 + 7\ Ru_4Si_3$	386
$6RuTa + 11\ Ru_2Si_3 \rightarrow 6TaSi_2 + 7Ru_4Si_3$	641
$2RuTa + 3Ru_2Si_3 \rightarrow Ta_2Si + 8RuSi$	20.8

$5RuTa + 8Ru_2Si_3 \rightarrow Ta_5Si_3 + 21RuSi$	50.3
$RuTa + 3Ru_2Si_3 \rightarrow TaSi_2 + 7RuSi$	59.3
$6RuTa + Ru_2Si_3 \rightarrow 3Ta_2Si + 8Ru$	583
$5RuTa + Ru_2Si_3 \rightarrow Ta_5Si_3 + 7\ Ru$	506
$RuTa + 2Ru_2Si \rightarrow TaSi_2 + 5Ru$	263
$2RuTa + 8Ta_5Si_3 \rightarrow 21Ta_2Si + Ru_2Si_3$	34.6
$Ta_5Si_3 + Ru_2Si_3 \rightarrow 2RuTa + 3TaSi_2$	127
Ta-Ru-O	
$5RuTa + 2Ta_2O_5 \rightarrow 9Ta + 5RuO_2$	3080
$4Ru + 2Ta_2O_5 \rightarrow 4RuTa + 5O_2$	2610
$9Ru + 2Ta_2O_5 \rightarrow 4RuTa + 2RuO_2$	3330
Ru-Ta-Si-O	
$4RuTa + 5SiO_2 \rightarrow 2Ta_2O_5 + 2RuSi + Ru_2Si_3$	375
$7RuTa + 7SiO_2 \rightarrow 7RuO_2 + Ta_5Si_3 + 2TaSi_2$	4380
$9SiO_2 + 2Ta_2O_5 + 14RuTa \rightarrow 14RuO_2 + 9Ta_2Si$	-8240
$7RuO_2 + 2Ta_2Si \rightarrow 2SiO_2 + 2Ta_2O_5 + 7Ru$	-3430
$RuO_2 + Ta_5Si_3 \rightarrow RuTa + SiO_2 + 2Ta_2Si$	-611
$37RuO_2 + 9Ta_5Si_3 \rightarrow 37RuTa + 27SiO_2 + 4Ta_2O_5$	-22000
$37RuO_2 + 4Ta_5Si_3 \rightarrow 10Ta_2O_5 + 12SiO_2 + 37Ru$	-18200
$3TaSi_2 + 5RuO_2 \rightarrow 5SiO_2 + 3RuTa + Ru_2Si$	-3130
$25TaSi_2 + 14RuO_2 \rightarrow 14SiO_2 + 5Ta_5Si_3 + 7Ru_2Si_3$	-9660
$5TaSi_2 + 7RuO_2 \rightarrow 7SiO_2 + 5RuTa + Ru_2Si_3$	-4510
$2TaSi_2 + 3RuO_2 \rightarrow 3SiO_2 + 2RuTa + RuSi$	-1930
$7TaSi_2 + 11RuO_2 \rightarrow 11SiO_2 + 7RuTa + Ru_4Si_3$	-7000
$TaSi_2 + 2RuO_2 \rightarrow 2SiO_2 + RuTa + Ru$	-1200
$4TaSi_2 + 13RuO_2 \rightarrow 8SiO_2 + 2Ta_2O_5 + 13Ru$	-6840
$6Ta_2O_5 + 5Ru_4Si_3 \rightarrow 15SiO_2 + 12RuTa + 8Ru$	-810
$2Ta_2O_5 + 3Ru_4Si_3 \rightarrow 5SiO_2 + 4RuTa + 4Ru_2Si$	-253
$2Ta_2O_5 + 5RuSi \rightarrow 5SiO_2 + 4RuTa + Ru$	-310
$2Ta_2O_5 + 6RuSi \rightarrow 5SiO_2 + 4RuTa + Ru_2Si$	-314
$2Ta_2O_5 + 8RuSi \rightarrow 5SiO_2 + 4RuTa + Ru_4Si_3$	-335
$8Ta_2O_5 + 7Ru_2Si_3 \rightarrow 20SiO_2 + 14RuTa + Ta_2Si$	-1480
$42Ta_2O_5 + 37Ru_2Si_3 \rightarrow 105SiO_2 + 2Ta_5Si_3 + 74RuTa$	-7780
$2Ta_2O_5 + 5Ru_2Si \rightarrow 5SiO_2 + 6Ru + 4RuTa$	-290
Ta-Si-N	
$6TaN + Si_3N_4 \rightarrow 3Ta_2Si + 5N_2$	951
$10TaN + 2Si_3N_4 \rightarrow 2Ta_5Si_3 + 9N_2$	1660
$6TaN + 4Si_3N_4 \rightarrow 6TaSi_2 + 11N_2$	1960
$TaN + 3Ta_2Si \rightarrow Ta_2N + Ta_5Si_3$	26
$7TaN + 2Ta_5Si_3 \rightarrow 7Ta_2N + 3TaSi_2$	344
$4TaN + Ta_5Si_3 \rightarrow Si_3N_4 + 9Ta$	590
$12TaN + 10TaSi_2 \rightarrow 11Ta_2Si + 3Si_3N_4$	220
$28TaN + 27TaSi_2 \rightarrow 11Ta_5Si_3 + 7Si_3N_4$	315
$Si_3N_4 + 4TaSi_2 \rightarrow 11Si + 4TaN$	131
$Si_3N_4 + 8TaSi_2 \rightarrow 19Si + 4Ta_2N$	456
$3Ta_2Si + 14TaN \rightarrow 10Ta_2N + Si_3N_4$	316

Si-N-O	
$2N_2 + 4SiO_2 \rightarrow 2Si_2N_2O + 3O_2$	1620
$2N_2 + 3SiO_2 \rightarrow Si_3N_4 + 3O_2$	1710
Ta-N-O	
$2Ta_2O_5 + 2N_2 \rightarrow 4TaN + 5O_2$	2440
$2Ta_2O_5 + N_2 \rightarrow 2Ta_2N + 5O_2$	2730
Ta-Si-N-O	
$52TaN + 55SiO_2 \rightarrow 22Ta_2O_5 + 13Si_3N_4 + 8TaSi_2$	7130
$14TaN + 16SiO_2 \rightarrow 5Ta_2O_5 + 7\ Si_2N_2O + 2Ta_2Si$	1360
$74TaN + 86SiO_2 \rightarrow 27Ta_2O_5 + 37Si_2N_2O + 4Ta_5Si_3$	7280
$26TaN + 34SiO_2 \rightarrow 11Ta_2O_5 + 13Si_2N_2O + 4TaSi_2$	3010
$14TaN + 10SiO_2 \rightarrow 3Ta_2O_5 + 5Si_2N_2O + 4Ta_2N$	987
$14Ta_2N + 5SiO_2 \rightarrow 5Ta_2Si + 2Ta_2O_5 + 14TaN$	-54.2
$3Ta_2O_5 + 5Si_2N_2O \rightarrow 10SiO\ 2 + 6TaN + 2N_2$	-402
$32Ta + 5Si_2N_2O \rightarrow Ta_2O_5 + 10TaN + 10Ta_2Si$	-1460
$6Ta_2O_5 + 5Si_3N_4 \rightarrow 15SiO_2 + 12TaN + 4N_2$	-1230
$3Ta_2O_5 + 10Si_3N_4 \rightarrow 15Si_2N_2O + 6TaN + 2N_2$	-1260
$26TaN + 55Si_2N_2O \rightarrow 11Ta_2O_5 + 34Si_3N_4 + 4TaSi_2$	5920
$10Ta_2N + 2Si_2N_2O \rightarrow 14TaN + SiO_2 + 3Ta_2Si$	-428
$9Ta_2N + 2Si_2N_2O \rightarrow 13TaN + SiO_2 + Ta_5Si_3$	-401
$11Ta_2N + 4Si_2N_2O \rightarrow 19TaN + 2SiO_2 + 3TaSi_2$	-459
$32Ta_2N + 5Si_2N_2O \rightarrow 42TaN + Ta_2O_5 + 10Ta_2Si$	-1100
$27Ta_2Si + 2Si_2N_2O \rightarrow 4TaN + SiO_2 + 10Ta_5Si_3$	-168
$11Ta_5Si_3 + 14Si_2N_2O \rightarrow 28TaN + 7SiO_2 + 27TaSi_2$	285
Ta-Ru-Zr	
$RuTa + RuZr \rightarrow Ru_2Zr + Ta$	117
$Ta + RuZr \rightarrow Zr + RuTa$	17.9
Ru-Zr-O	
$Ru + ZrO_2 \rightarrow RuO_2 + Zr$	765
$3Ru + ZrO_2 \rightarrow RuO_2 + Ru_2Zr$	635
$2Ru + ZrO_2 \rightarrow RuO_2 + RuZr$	632
$2RuO_2 + ZrO_2 \rightarrow Ru_2Zr + 3O_2$	971
$RuO_2 + ZrO_2 \rightarrow RuZr + 2O_2$	856
Ta-Zr-O	
$4Ta + 5ZrO_2 \rightarrow 2Ta_2O_5 + 5Zr$	1310
Ru-Ta-Zr-O	
$2Ta_2O_5 + 5RuZr \rightarrow 5ZrO_2 + 4RuTa + Ru$	-1110
$2Ta_2O_5 + 6RuZr \rightarrow 5ZrO_2 + 4RuTa + Ru_2Zr$	-1110
$2Ta_2O_5 + 5Ru_2Zr \rightarrow 5ZrO_2 + 4RuTa + 6Ru$	-1120